An efficient cluster elongation method in density functional theory and its application to polyhydrogenbonding molecules

Yuriko Aoki, Sándor Suhai, and Akira Imamura

Citation: The Journal of Chemical Physics **101**, 10808 (1994); doi: 10.1063/1.468479
View online: http://dx.doi.org/10.1063/1.468479
View Table of Contents: http://scitation.aip.org/content/aip/journal/jcp/101/12?ver=pdfcov
Published by the AIP Publishing

An efficient cluster elongation method in density functional theory and its application to poly-hydrogen-bonding molecules

Yuriko Aoki[a] and Sándor Suhai
Department of Molecular Biophysics, Deutsches Krebsforschungszentrum, Neuenheimer Feld 280, D-69120 Heidelberg, Germany

Akira Imamura
Department of Chemistry, Faculty of Science, Hiroshima University, Kagamiyama 1-3, Higashi-Hiroshima 724, Japan

(Received 23 May 1994; accepted 16 September 1994)

The elongation method to synthesize the electronic states of polymers is developed at the level of the density functional theory using the linear combination of Gaussian-type orbitals local spin density method. In this treatment, the interactions between the localized molecular orbitals of a cluster and the canonical molecular orbitals of an attacking monomer are successively included, where the Kohn–Sham equation is self-consistently solved instead of the Hartree–Fock equation in the conventional *ab initio* method. In the process of the cluster extension, an efficient treatment is implemented to calculate the matrix elements of Coulomb integral and exchange-correlation potential. The reliability and the efficiency of this method are examined via applications to hydrogen molecule cluster, linear water cluster $(H_2O)_n$ and formamide cluster $(CHONHH_2)_n$. It was shown that the present method saves significantly the computational time and disk storage in the large cluster calculations, and provides good agreements with the results by the conventional density functional treatment for the whole system. © *1994 American Institute of Physics.*

I. INTRODUCTION

We are developing the elongation method,[1] a new theoretical approach to obtain electronic states of large clusters, treating only a few units at a time of the total system. The canonical wave function of a so-called starting cluster is localized, the interaction between this cluster and an attacking monomer included, followed by localization of the new wave function and so on. The elongation method was applied to various systems such as polyethylene and polypropylene at the level of the extended Hückel method, and the total energies and electron densities thus obtained are in good agreement with the results obtained by the conventional diagonalization method.

The aforementioned elongation method can be performed with a constant number of molecular orbitals and also constant dimension of Fock matrix. Therefore, this leads to great saving in the computations at the level of semiempirical treatments such as extended Hückel, CNDO/2, MNDO methods, and so on, in which the Fock matrix diagonalization, which is an N^3 procedure, dominates the calculation. On the other hand, in most *ab initio* methods the two-electron integral evaluation which is an N^4 procedure dominates the computation time and thus the Fock matrix diagonalization is not so time consuming compared with the two-electron integral part. As the number of atoms and electrons in the system increases, the N^4 problem rapidly exceeds the capacity of even the most advanced present-day computer. Therefore, in the viewpoint of developing a powerful strategy toward large molecules, it is useless to apply the elongation method to *ab initio* level unless the integral problem is overcome.

In recent years, density functional theory (DFT) based on the Hohenberg–Kohn–Sham theory[2,3] was remarkably developed and many applications were performed in the area of molecular structure and properties. Owing to the great simplifications in the treatment of exchange and correlation effects, there has been a significant increase in the applications for large clusters including transition-metal, organometallic systems, and so on. However, in the basic density functional Kohn–Sham self-consistent-field (KS-SCF) calculation, there are two bottlenecks for the application to large polymer systems. The first is the evaluation of the two-electron integrals. Although this is the same problem as is in most *ab initio* methods, the DFT is accessible with N^3M [N, the number of atomic orbitals (AO's); M, the number of the auxiliary functions) dependency in current implementations using another M fitting functions for charge density.[4–6] The second is the computational efforts in the exchange correlation (XC) potential over the grid points around each atom. However, the formalism for the XC potential is greatly simplified in the DFT, which makes it easy to treat so large molecules that cannot be dealt with the more sophisticated formalisms including electron correlations based on the conventional Hartree–Fock method.

Under such circumstances in quantum chemical methodologies, we are developing the elongation method by combining the DFT toward the more powerful methodology for large systems like DNA or protein in biopolymers. The program package DeMon, which was developed by St-Amant and Salahub,[7,8] was used for the combination. This approach is based on the linear combination of the Gaussian-type orbitals local spin density (LCGTO-LSD) method originally suggested by Sambe and Felton[4] and further developed by

[a]Present address: Department of Chemistry, Faculty of Science, Hiroshima University, Kagamiyama 1-3, Higashi-Hiroshima 724, Japan.

 0021-9606/94/101(12)/10808/16/$6.00

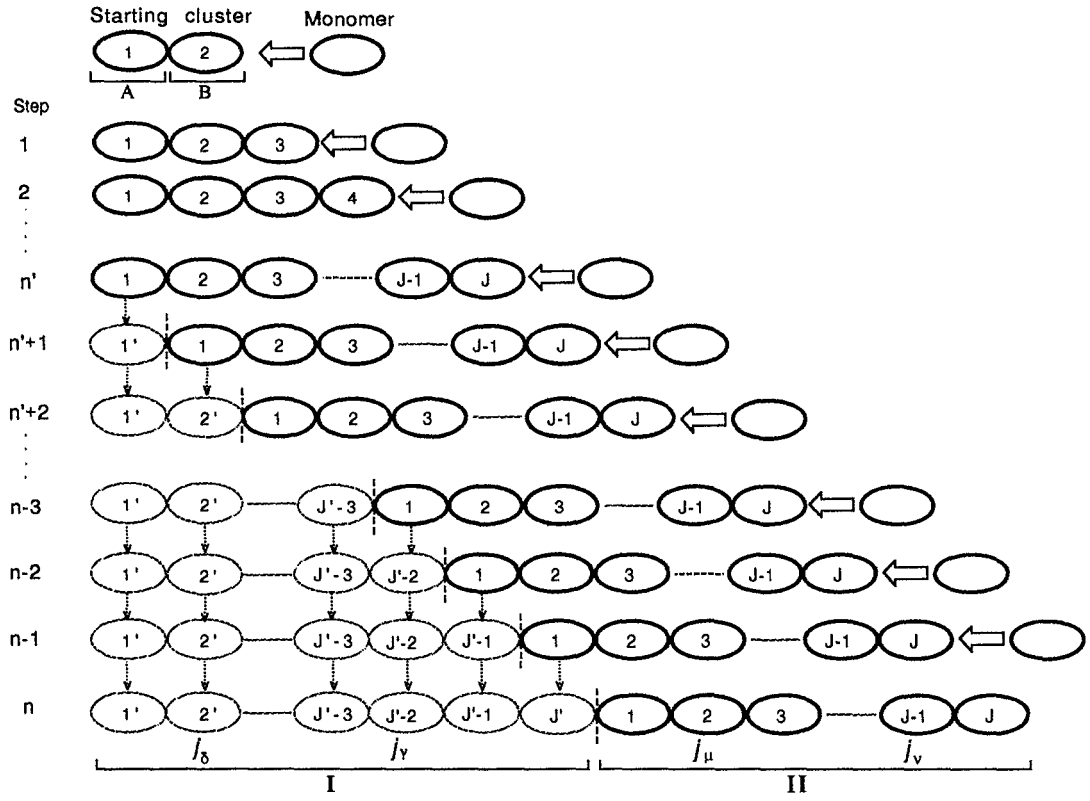

FIG. 1. Schematic illustration for the elongation method.

Dunlap *et al.*[5,6] and by others. In our previous work,[9] we have used the analytical treatment for the evaluations of the Coulomb and XC potentials, in which constant number of the fitted basis for XC potential was employed during the elongation. However, in this treatment, the Fock matrix was not properly described for the whole cluster, leading to some slight errors in the total energies. In the present work, therefore, analytical treatment in Coulomb integrals is performed with M dependency, but numerical evaluation in XC potential is implemented with the constant number of grid points during cluster elongation. The numbers of the AO's and MO's employed are also retained to be constant regardless of the increase of the cluster size. The efficiency and the reliability of this method are demonstrated by applying it to poly-hydrogen-bonding molecules. However, we will not discuss in detail on the absolute values obtained, because our purpose of the present work is to examine the applicability of our method as a first step in comparison with the conventional DFT method.

In Sec. II we review our methodology implemented in the combination between the elongation method and the DFT method. In Sec. III, as the first step to examine the efficiency and accuracy of our treatment, the calculations are carried out for a regularly arranged hydrogen molecule cluster. Next, applications are performed for the elongation of water clusters with using various lengths of starting cluster. The accuracy of our results and the computational requirements are discussed, compared to those by the conventional DFT treatment. Finally, to investigate the applicability to the more complicated systems, the method is carried out for formamide linear chains.

II. METHOD

The elongation method is already reviewed in our previous papers, and we display here equations germane to the subsequent development of the computational method. In the following the process of our treatment is described according to Fig. 1.

Initially, a starting cluster composed of appropriate number of monomer units is calculated by the usual LCGTO-LSD method. The canonical molecular orbitals (CMO's) of this cluster, $\{\psi_i^\sigma\}$, are given by

$$\psi_i^\sigma = \sum_{\mu}^{\text{on } j_\mu} \sum_{j_\mu=1}^{N_s} C_{\mu i}^{j_\mu \sigma} \chi_\mu^{j_\mu} \quad (i=1,2,3,\ldots,m) \tag{1}$$

as a one-electron orbital for the usual DFT one-electron Hamiltonian

$$H = -\tfrac{1}{2}\nabla^2(1) - \sum_p Z_p / r_{1p} + V_c(1) + V_{XC}(1). \tag{2}$$

In Eq. (1), $\chi_\mu^{j_\mu}$ indicates the μth atomic orbital (AO) that belongs to the j_μth cell of the cluster. N_s is the number of the cells taken as the starting of the elongation (two cells are adopted in the Fig. 1). The cluster is then divided into two

regions, A and B, with the assumption that a new monomer is added to the end of B. The region A is the furthest molecule moiety from the attacking molecule. Next, particular CMO's $\{\psi_i^\sigma; i=1,2,\ldots,m_A\}$ are localized in the region A and the others, $\{\psi_i^\sigma; i=m_A+1,\ldots,m_A+m_B\}$, in the region B. The resulting LMO's are expressed on the basis of AO's μ and ν as

$$\phi_i^\sigma(A)=\sum_{j_\mu=1}^{J}\sum_{\mu}^{\text{on } j_\mu} L_{\mu i}^{j_\mu\sigma}(A)\chi_\mu^{j_\mu} \quad (i=1,2,\ldots,m_A) \tag{3}$$

$$\phi_i^\sigma(B)=\sum_{j_\mu=1}^{J}\sum_{\mu}^{\text{on } j_\mu} L_{\mu i}^{j_\mu\sigma}(B)\chi_\mu^{j_\mu} \quad (i=1,2,\ldots,m_B). \tag{4}$$

For details of the expressions refer to Ref. 1. In the present work, applying to poly-hydrogen molecules, the LMO's are more efficiently obtained by the following treatment. That is, the coefficients $L_{\mu i}^{j_\mu\sigma}$ (written by $L_{\mu i}^{\sigma}$ in the following because the μth AO belongs usually to the j_μth cell) are given by the unitary transformation

$$L_{\mu i}^{\sigma}=\sum_{j}^{m} C_{\mu j}^{\sigma'}U_{ji}, \tag{5}$$

so as to give the maximum value of

$$S_{ij}^{AB}=\sum_{\mu}^{\text{on } A}\sum_{\nu}^{\text{on } A} C_{\mu j}^{\sigma'}C_{\nu i}^{\sigma'}+\sum_{\mu}^{\text{on } B}\sum_{\nu}^{\text{on } B} C_{\mu j}^{\sigma'}C_{\nu j}^{\sigma'}, \tag{6}$$

where $C_{\mu j}^{\sigma'}$ is a coefficient of the orthogonalized AO in CMO, which is obtained by the symmetric transformation matrix X and given by

$$C_{\mu j}^{\sigma'}=\sum_{\nu}^{\text{on } A+B}\sum_{\rho}^{\text{on } A+B} S_{\mu\nu}X_{\nu\rho}C_{pj}^{\sigma}. \tag{7}$$

For the inclusion of the interaction with attacking monomer $\{\psi_i^\sigma(M); i=1,2,\ldots,m_M\}$, the LMO's $\phi_i^\sigma(A)$ are removed and only $\phi_j^\sigma(B)$ and $\psi_i^\sigma(M)$ are treated in the diagonalization. The newly obtained CMO's are again localized in the region A and region B using Eqs. (3) and (4), respectively, and then $\phi_j^\sigma(B)$ and $\psi_i^\sigma(M)$ interacted, followed by localization and so on. This procedure is repeated by including subsequently the interaction between cluster and attacking monomer. The Kohn–Sham (KS) equation performed in the process is given by

$$\sum_{j=1}^{m} F_{ij}^{\sigma(n)}U_{kj}^{\sigma(n)}=\epsilon_i^{\sigma(n)}\sum_{j=1}^{m} S_{ij}^{(n)}U_{kj}^{\sigma(n)} \quad (m=m_B+m_M), \tag{8}$$

where S_{ij} is a matrix element of overlap integrals on the basis of the LMO of cluster or the CMO of attacking monomer. $F_{ij}^{\sigma(n)}$ is a σ spin Fock matrix element also based on the LMO or CMO and is written by

$$F_{ij}^{\sigma(n)}(i,j=1,2,\ldots,m_B)=\sum_{j_\mu=1}^{J}\sum_{j_\nu=1}^{J}\sum_{\mu=1}^{\text{on } j_\mu}\sum_{\nu=1}^{\text{on } j_\nu} L_{\mu i}^{\sigma(n)}(B)\times F_{\mu\nu}^{\sigma(n)}L_{\nu j}^{\sigma(n)}(B), \tag{9}$$

$$F_{ij}^{\sigma(n)}(i,j=m_B+1,2,\ldots,m)=\epsilon_i^{(n)}(M)\,\delta_{ij}, \tag{10}$$

$$F_{ij}^{\sigma(n)}(i=1,2,\ldots,m_B,j=m_B+1,\ldots,m)=\sum_{j_\mu=1}^{J}\sum_{\mu=1}^{\text{on } j_\mu}\sum_{\chi=1}^{\text{on } M} L_{\mu i}^{\sigma(n)}(B)F_{\mu\chi}^{\sigma(n)}C_{\chi j}^{\sigma(n)}(M). \tag{11}$$

In Eq. (9), $L_{\mu i}^{\sigma(n)}(B)$ means the ith energy level for the coefficient of the LMO given by Eq. (4) at the step n and gives nonvanishing matrix elements between occupied orbitals or between vacant orbitals. $\epsilon_i^{(n)}(M)$ in Eq. (10) means the ith energy level for the canonical orbital of the monomer attacking at step n. The interaction between the polymer and the monomer is incorporated by Eq. (11), in which $C_{\chi j}^{\sigma(n)}(M)$ means a coefficient of the CMO's of the monomer attacking at step n.

$F_{\mu\nu}^{\sigma(n)}$ is given in the framework of the density functional theory by

$$F_{\mu\nu}^{\sigma(n)}=h_{\mu\nu}^{(n)}+F_{\mu\nu}^{C(n)}+F_{\mu\nu}^{\text{xc}\sigma(n)}, \tag{12}$$

where the first term is core Hamiltonian matrix element, the second and third ones are the Coulomb repulsion and exchange-correlation potentials, respectively, given by

$$F_{\mu\nu}^{C(n)}=(\mu\nu|r_{12}^{-1}|\tilde{\rho}^{(n)}), \tag{13}$$

and

$$F_{\mu\nu}^{xc(n)}=\langle\mu|\nu_{xc}^{\sigma}|\nu\rangle^{(n)}. \tag{14}$$

Charge density (CD), ρ, is fitted for the total system including J cells in the same manner as in the conventional density functional treatment by

$$\rho(r)^{(n)}\cong\tilde{\rho}(r)^{(n)}=\sum_{j_\lambda=1}^{J}\sum_{\lambda=1}^{\text{on } j_\lambda} a_\lambda^{j_\lambda(n)}f_\lambda^{j_\lambda}, \tag{15}$$

where $f_\lambda^{j_\lambda}$ is an auxiliary basis belonging to the j_λth cell given by an LCGTO. The set of coefficients for fitting ρ, $\{a_\lambda\}$, is obtained by a least square fitting (LSF) procedure which minimizes the error in the Coulomb repulsion energy

$$[\rho(1)^{(n)}-\tilde{\rho}(1)^{(n)}|1/r_{12}|\rho(2)^{(n)}-\tilde{\rho}(2)^{(n)}], \tag{16}$$

while maintaining charge conservation.[5,6] The ρ is defined from the LMO's as

$$\rho^{(n)}=\sum_{i}^{\text{occ}} n_i^\alpha|\phi_i^{\alpha(n)}(A)+\phi_i^{\alpha(n)}(B)|^2+\sum_{i}^{\text{occ}} n_i^\beta|\phi_i^{\beta(n)}(A)+\phi_i^{\beta(n)}(B)|^2, \tag{17}$$

where n_i^α and n_i^β are occupation numbers of the ith α and β spin orbitals, respectively. Only the LMO's localized in the B region are changed during self-consistent-field (SCF) procedure.

On the other hand, the XC potential must be calculated over a set of grid points centered about each atom because of its $\rho(1)^{1/3}$ dependency. Analytical treatment for the matrix elements of the XC potential is proposed by Sambe and Felton,[3] developed by Dunlap,[4,5] and also available in the DeMon program. However, in the analytical treatment not only grid points around every atom, but also auxiliary functions are used for fitting the potential. This makes it quite difficult to drop out the grid points which belong to the part I (after the step n' in Fig. 1 as mentioned afterwards). Therefore, in the present work, the matrix elements of the XC potential, given by Eq. (14), are evaluated by the numerical sampling of grid points around the atoms.

Up to this stage, the Fock matrix elements included in the Kohn–Sham equation are calculated explicitly for the whole system. After several cycles (n' step in Fig. 1), however, the AO's $\chi_\mu^{j_\mu}$ ($j_\mu=1$) belonging to the terminal cell can be dropped under the condition that the coefficients of the LMO ϕ_j^σ ($j=1,2,\ldots,m$) on the terminal cell become negligibly small and then

$$\Delta S_{ii}^{\sigma(n)}=\sum_{\mu}^{\text{on } j_\mu=1}\sum_{\nu}^{\text{on } j_\nu=1} L_{\mu i}^{\sigma(n)}(X)L_{\nu i}^{\sigma(n)}(X)S_{\mu\nu}\leqq\delta \quad (i=1,2,\ldots,m,\quad X=A,B). \tag{18}$$

This means that the m LMO's which are employed in the Kohn–Sham equation, Eq. (8), do not have any more contributions on the terminal cell. The density matrix on the terminal AO's satisfying the aforementioned condition is therefore unaltered in the subsequent cycles in the case of the one-directional extension. In the present work, $\delta=10^{-8}$ is adopted for the criterion. We define the removed part as part I and the remaining part as part II. The coefficients of the LMO's in part I become inactive for the approaching attacking monomer and, therefore, unchanged in the subsequent cycles. On the other hand, those in the part II are reactive with the attacking monomer, and therefore should be treated explicitly. By this treatment the number of the cells included in part I ($1',2',\ldots,J'$) increases with the elongation cycles, while that in part II ($1,2,\ldots,J$) remains to be generally constant as shown in Fig. 1. This means that only the Fock matrix elements belonging to the part II (J cells) can be employed in the SCF diagonalization procedure at each elongation step. This leads to much saving in computational time and disk storage. From this standpoint, for the step n ($>n'$), the KS equation is represented by

$$\sum_{j=1}^{m} F_{kj}^{\sigma(n)}(II)U_{ij}^{\sigma(n)}(II)=\epsilon_i^{\sigma(n)}\sum_{j=1}^{m} S_{kj}^{(n)}(II)U_{ij}^{\sigma(n)}(II). \tag{19}$$

$F_{kj}^{\sigma(n)}(II)$ is given by the same manner as Eqs. (9)–(11), but is written by the form

$$F_{\mu\nu}^{\sigma(n)}(II)=h_{\mu\nu}^{(n)}(II)+F_{\mu\nu}^{C(n)}(II)+F_{\mu\nu}^{xc\sigma(n)}(II) \tag{20}$$

instead of Eq. (12). The notation (II) means that the AO's μ and ν belong to part II. It is a serious problem how to evaluate exactly the second and third terms (two electron parts) without part I. Because many-center integrals (more than two-centers) should be evaluated for all the interactions among the AO's μ and ν in part II and the AO's δ and γ in part I, those terms concerned with μ and ν cannot be independently calculated regardless of part I (from now on, as shown in Fig. 1, we define the AO which belongs to part II as μ or ν and that to part I as δ or γ). In the density functional treatment developed by Dunlap *et al.*, instead of AO's δ and γ in part I, auxiliary functions are employed in the evaluation of Coulomb integrals [the second term in Eq. (20)] as written by Eq. (13). On the other hand, in the XC potential [the third term in Eq. (20)], grid points can be regarded as another basis for the electron density in part I. In the following, an efficient treatment for the Coulomb and XC potentials after step n' is described.

A. Coulomb integral

Coulomb repulsive term on the basis of AO's μ and ν is given, as well as Eq. (13), by

$$F_{\mu\nu}^{c(n)}(II)=(\mu\nu|r_{12}^{-1}|\tilde{\rho}^{(n)}), \tag{21}$$

where the AO's are reduced to those inside the area defined as part II. However, in the aforementioned, the CD potential is fitted using all of the auxiliary functions located on the $J+J'$ cells by

$$\rho(r)^{(n)}\cong\tilde{\rho}(r)^{(n)}=\sum_{j_\lambda=1}^{J+J'}\sum_{\lambda=1}^{\text{on } j_\lambda} a_\lambda^{j_\lambda(n)}f_\lambda^{j_\lambda}. \tag{22}$$

The long-range Coulomb interactions with the attacking monomer are evaluated through the coefficients $a_\lambda^{j_\lambda(n)}$ for the whole system. In the usual manner,[10] subjecting to the constraint

$$N_e=\sum_{j_\lambda=1}^{J'+J}\sum_{\lambda}^{\text{on } j_\lambda} a_\lambda^{j_\lambda(n)}\int f_\lambda dr=a\cdot n, \tag{23}$$

the matrix equation for the fit coefficients is then

$$a_\lambda^{j_\kappa(n)}=\sum_{j_\kappa=1}^{J'+J}\sum_{\kappa}^{\text{on } j_\kappa}[S^{-1}]_{\lambda\kappa}(t_\kappa^{(n)}+\Lambda n_\kappa), \tag{24}$$

where S^{-1} is the inverse matrix of the overlap integrals between auxiliary functions λ and κ, and Λ is the Lagrange multiplier. The $t_\lambda^{(n)}$ (t vector) is defined as

$$t_\lambda^{j_\lambda(n)}=\int \rho(1)^{(n)}f_\lambda^{j_\lambda}(2)/r_{12}dr_1dr_2. \tag{25}$$

This means that the fitting coefficients $a_\lambda^{j_\lambda(n)}$ should be determined through the t vector defined from the enormous number of two-electron integrals for the whole system. To circumvent this difficulty, in the elongation process we calculate the t vector according to the following manner.

The t vector can be divided into the two types of the contributions as

$$t_\lambda^{(n)}=t_\lambda^{(n)}(\in II)+t_\lambda^{(n)}(\notin II). \tag{26}$$

The first term whose AO's belong only to part II is directly calculated by the form

$$t_\lambda^{(n)}(\in II)=\frac{1}{2}\sum_{j_\mu=1}^{J}\sum_{j_\nu=1}^{J}\sum_{\mu}^{\text{on } j_\mu}\sum_{\nu}^{\text{on } j_\nu} P_{\mu\nu}^{(n)}[\mu\nu|r_{12}^{-1}|f_\lambda]. \tag{27}$$

The second term in the right-hand side of Eq. (26) is the contribution of the AO's from other than part II and, furthermore, divided into the two contributions composed of the auxiliary functions on the cells $1'\sim J-1$ and on the cell J.

$$t_\lambda^{(n)}(\notin II)\cong t_\lambda^{(n-1)}(\notin II,1'\sim J-1)+t_\lambda^{(n-1)}(\notin II,J). \tag{28}$$

The first contribution is written by

$$\begin{aligned} &t_\lambda^{(n-1)}(\notin II,1'\sim J-1)\\ &=\frac{1}{2}\sum_{j_\delta=1}^{J'}\sum_{j_\gamma=1}^{J'}\sum_{\delta}^{\text{on } j_\delta}\sum_{\gamma}^{\text{on } j_\gamma} P_{\delta\gamma}^{(n-1)}\\ &\times[\delta\gamma|r_{12}^{-1}|f_\lambda(j_\lambda\in 1'\sim J',1\sim J-1)]\\ &+\sum_{j_\delta=1}^{J'}\sum_{j_\mu=1}^{J-1}\sum_{\delta}^{\text{on } j_\delta}\sum_{\mu}^{\text{on } j_\mu} P_{\delta\mu}^{(n-1)}\\ &\times[\delta\mu|r_{12}^{-1}|f_\lambda(j_\lambda\in 1'\sim J',1\sim J-1)] \end{aligned} \tag{29}$$

and already given as a one-dimensional vector from the previous step, and therefore those terms do not have to be any more recalculated. The second contribution in Eq. (28) is the integrals between the AO with respect to the part I dropped out already and the auxiliary function on the cell J added newly at the step n, and written by

$$\begin{aligned} &t_\lambda^{(n-1)}(\notin II,J)\\ &=\frac{1}{2}\sum_{j_\delta=1}^{J'}\sum_{j_\gamma=1}^{J'}\sum_{\delta}^{\text{on } j_\delta}\sum_{\gamma}^{\text{on } j_\gamma} P_{\delta\gamma}^{(n-1)}[\delta\gamma|r_{12}^{-1}|f_\lambda(j_\lambda\in J)]\\ &+\sum_{j_\delta=1}^{J'}\sum_{j_\mu=1}^{J}\sum_{\delta}^{\text{on } j_\delta}\sum_{\mu}^{\text{on } j_\mu} P_{\delta\mu}^{(n-1)}[\delta\mu|r_{12}^{-1}|f_\lambda(j_\lambda\in J)]. \end{aligned} \tag{30}$$

Although these terms are small corrections for the long range interactions, we cannot ignore them to obtain exact t vector. As a result, only the contributions in part II given by Eq. (27) must be explicitly calculated and a few terms given by Eq. (30) are added as well. On the other hand, the contributions from part I given by Eq. (29) can be transformed as a one-dimensional vector from the previous step without any further calculations in the subsequent cycles. That is to say, all of the information on the two-electron integrals in part I are stored as a t vector and transferred intact to the next elongation step. By this treatment the two-electron integrals, proportional to N^2M in the usual LCGTO-LSD method, can be reduced to those proportional to $\sim M$. In the above process, the number of the AO's in part II remains to be constant and only the number of auxiliary functions increases with the size of the cluster. The aforementioned treatment using the t vector makes it possible to evaluate Coulomb interactions efficiently without direct calculations of the two-electron integrals for the whole system in the process of elongation. Furthermore, strong Coulomb interactions, as observed in biopolymers, can be evaluated with good accuracy, because the LSF procedure for fitting the potential is performed on the whole system.

B. XC potential

Fortunately, the DFT enables us to treat the XC potential only within part II because of its simplicity. In our previous work,[9] in which analytical treatment was used without grid points in part I, well fitted potentials could not be obtained. This caused an end effect near the surface between part I and part II, which led to some slight errors in the total energies. To avoid this difficulty, in the present work, we have used numerical integrations for the evaluation of the matrix elements of XC potential. The third term of Eq. (20), based on the AO's μ and ν inside part II, is divided into two terms as

$$F_{\mu\nu}^{\text{XC}\sigma(n)}(II)=\langle\mu|\nu_{\text{XC}}^{\sigma(II)}|\nu\rangle^{(n)}+\langle\mu|\nu_{\text{XC}}^{\sigma(I)}|\nu\rangle^{(n)}. \tag{31}$$

The first term, the contribution from the potential in part II, is represented by

$$\langle\mu|\nu_{\text{XC}}^{\sigma(II)}|\nu\rangle^{(n)}=\sum_{j_p=1}^{J}\langle\mu|\nu_{\text{XC}}^{\sigma}|\nu\rangle_{j_p}^{(n)}, \tag{32}$$

where j_p means the cell on which pth atom is located. The matrix element of the potential with respect to the cell j_p is given as the summation of the XC potential over all the grid points included in the cell j_p by

$$\langle\mu|\nu_{\text{XC}}^{\sigma}|\nu\rangle_{j_p}=\sum_{p}^{\text{on } j_p}\sum_{k}^{\text{on } p} w(r_k)\chi_\mu(r_k)\nu_{\text{XC}}^{\sigma}(\rho^\sigma(r_k))\chi_\nu(r_k). \tag{33}$$

The r_k is a grid point centered about the pth atom in the jth cell and $w(r_k)$ is an arbitrary weight which may be assigned to the r_kth point. In generating these values of weight s, the DeMon uses Becke's approach[11] to decomposing the molecular integration into a sum of one-center atomlike integrations. It should be noticed in the elongation method that the arbitrary weights should be assigned so as to include the effect of overlapping atom-centered grids in the molecule. Therefore, the weight on the pth atom of the j_pth cell of part II, should be determined under the existence of the atoms included in the part I. The XC potential on the grid point r_k in Eq. (33) is a function of the electron density on the grid point r_k

$$\rho^\sigma(r_k)=\sum_{i}^{\text{occ}}|\psi_i^\sigma(r_k)|^2, \tag{34}$$

where the wave functions on the grid point r_k are given by

$$\begin{aligned} \psi_i^\sigma(r_k)=&\sum_{j_\mu=1}^{J'}\sum_{\mu}^{\text{on } j_\mu}\chi_\mu(r_k)C_{\mu i}^\sigma(\in II)\\ &+\sum_{j_\delta=1}^{J'}\sum_{\delta}^{\text{on } j_\delta}\chi_\delta(r_k)C_{\delta i}^\sigma(\in I). \end{aligned} \tag{35}$$

The definition of Eq. (32) means that only the r_k's within part II are used in Eqs. (34) and (35). However, the summa-

tion on δ in the second term in Eq. (35) should be run over all the AO's in part I with respect to every r_k. This part needs more computer time as the cluster becomes long in the elongation process. However, it is very important for describing exactly the potential as well as the electron density near part I. Additionally, for the nonlocal corrections in the XC potential, the terms $\Delta\psi_i^\sigma(r_k)$ and $\Delta^2\psi_i^\sigma(r_k)$ for Eq. (35) also should be calculated by summing over all the AO's μ and δ.

The second term in Eq. (31) means the contribution from the potential located in part I and given by

$$\langle\mu|\nu_{\mathrm{XC}}^{\sigma(I)}|\nu\rangle^{(n)}=\sum_{j_p=1}^{J'}\langle\mu|\nu_{\mathrm{XC}}^{\sigma}|\nu\rangle_{j_p}^{(n)}, \tag{36}$$

where the subscript j_p means the contribution from the j_pth cell in the XC potential as given by Eq. (33). That is, the matrix element in part I is given by summing up the potentials on all the grid points not only in part II but also in part I. Those calculations on the basis of grid points are the most time consuming part in the density functional treatment and need much CPU time if these values are directly calculated for the whole system. We can avoid this difficulty by introducing the following approximation:

$$\langle\mu|\nu_{\mathrm{XC}}^{\sigma}|\nu\rangle_{j_p=J'}^{(n)}\cong\langle\mu|\nu_{\mathrm{XC}}^{\sigma}|\nu\rangle_{j_p=1}^{(n-1)},$$

$$\langle\mu|\nu_{\mathrm{XC}}^{\sigma}|\nu\rangle_{j_p=J'-1}^{(n)}\cong\langle\mu|\nu_{\mathrm{XC}}^{\sigma}|\nu\rangle_{j_p=1}^{(n-2)},$$

$$\vdots$$

$$\langle\mu|\nu_{\mathrm{XC}}^{\sigma}|\nu\rangle_{j_p=1'}^{(n)}\cong\langle\mu|\nu_{\mathrm{XC}}^{\sigma}|\nu\rangle_{j_p=1}^{(n')}.$$

This means that the matrix element between AO's μ and ν on the potential of $j_p=J'$ (the end cell of part I) at the step n is nearly equal to that on the potential of $j_p=1$ (the first cell of part II) at the previous step $n-1$. By summing up those relations, it is clear that the right-hand side of the Eq. (36) results in

$$\langle\mu|\nu_{\mathrm{XC}}^{\sigma(I)}|\nu\rangle^{(n)}\cong\sum_{m=n'}^{n-1}\langle\mu|\nu_{\mathrm{XC}}^{\sigma}|\nu\rangle_{j_p=1}^{(m)}. \tag{37}$$

The summation can be automatically performed by saving the contribution of the potential on the first cell ($j_p=1$) at each step m. This manipulation makes it possible to evaluate nearly exact matrix elements, Eq. (31), without recalculating directly the contribution from part I, Eq. (36). This leads to the great saving in the computations over the considerable number of grid points. As a result, the Fock matrix element to be employed after the step n' is represented as

$$F_{\mu\nu}^{\mathrm{XC}(n)}(II)\cong\sum_{j_p=1}^{J}\langle\mu|\nu_{\mathrm{XC}}^{\sigma}|\nu\rangle_{j_p}^{(n)}+\sum_{m=n}^{n-1}\langle\mu|\nu_{\mathrm{XC}}^{\sigma}|\nu\rangle_{j_p=1}^{(m)} \tag{38}$$

C. Total energy

Finally, the total energy is represented at the step n by

$$E^{(n)}=h^{(n)}+U_c^{(n)}+U_{\mathrm{XC}}^{(n)}+\mathrm{N.R.} \tag{39}$$

The first term includes the matrix elements of the kinetic energy and the nuclear-electron attraction [corresponding to the first and the second terms of the one-electron Hamiltonian in Eq. (2), respectively]. The nuclear-electron attraction terms are calculated for the whole system in the elongation cycle.

The second term in Eq. (39) is Coulomb energy which is given by

$$U_c^{(n)}=2\tilde{U}_c^{(n)}-\tilde{\tilde{U}}_c^{(n)}. \tag{40}$$

The first term is the Coulomb repulsion between the fitted density [given by Eq. (15)] and the density matrix from LMO's for the whole cluster [given by Eq. (17)]. In the present work, since the one-dimensional vectors a_λ and t_λ are exactly given by the process of Eqs. (24)–(30), this term can be readily calculated by the inner-product between the two vectors.

$$\tilde{U}_c^{(n)}=\sum_{j_\lambda=1}^{J+J'}\sum_{\lambda}^{\text{on } j_\lambda}a_\lambda^{j_\lambda(n)}t_\lambda^{j_\lambda(n)}=a\cdot t. \tag{41}$$

Using the fitting coefficients by Eq. (24), the second term in Eq. (40) is also calculated for the total system by

$$\tilde{\tilde{U}}_c^{(n)}=\frac{1}{2}\sum_{j_\kappa=1}^{J'+J}\sum_{j_\lambda=1}^{J'+J}\sum_{\kappa=1}^{\text{on } j_\kappa}\sum_{\lambda=1}^{\text{on } j_\lambda}a_\kappa^{j_\kappa(n)}S_{\kappa\lambda}^{(j_\kappa j_\lambda)}a_\lambda^{j_\lambda(n)}, \tag{42}$$

where $S_{\kappa\lambda}^{(j_\kappa j_\lambda)}$ is an overlap integral between auxiliary functions κ on the j_κth cell and λ on the j_λth cell.

The third term in Eq. (39), the XC potential energy, is given by

$$U_{\mathrm{XC}}^{(n)}=U_{\mathrm{XC}}^{(n)}(\in II)+U_{\mathrm{XC}}^{(n)}(\notin II). \tag{43}$$

In the frame work of the LSD approximation, the first term whose AO's belong to part II is given by

$$U_{\mathrm{XC}}^{(n)}(\in II)\cong\sum_{j_\mu=1}^{J}\sum_{j_\nu=1}^{J}\sum_{\mu=1}^{\text{on } j_\mu}\sum_{\nu=1}^{\text{on } j_\nu}P_{\mu\nu}^{(n)}\times\left(\sum_{j_p=1}^{J}\langle\mu|\epsilon_{\mathrm{XC}}|\nu\rangle_{j_p}^{(n)}+\sum_{m=n'}^{n-1}\langle\mu|\epsilon_{\mathrm{XC}}|\nu\rangle_{j_p=1}^{(m)}\right), \tag{44}$$

where the term in the large parentheses is the energy matrix for the XC potential, and the relation

$$\langle\mu|\epsilon_{\mathrm{XC}}^{\sigma}(I)|\nu\rangle^{(n)}\cong\sum_{m=n'}^{n-1}\langle\mu|\epsilon_{\mathrm{XC}}^{\sigma}|\nu\rangle_{j_p=1}^{(m)}$$

is assumed as is the matrix element of the XC potential given by Eq. (37). The second term of the Eq. (43), the contribution of the AO's from other than part II, is given by

$$U_{\mathrm{XC}}^{(n)}(\notin II) \cong \sum_{j_\delta=1}^{J'} \sum_{j_\gamma=1}^{J'} \sum_{\delta=1}^{\text{on } j_\delta} \sum_{\gamma=1}^{\text{on } j_\gamma} P_{\delta\gamma}^{(n-1)} \langle \delta | \epsilon_{\mathrm{XC}}^{\sigma} | \gamma \rangle^{(n-1)} + 2 \sum_{j_\delta=1}^{J'} \sum_{j_\mu=1}^{J-1} \sum_{\delta=1}^{\text{on } j_\delta} \sum_{\mu=1}^{\text{on } j_\mu} P_{\delta\mu}^{(n-1)} \langle \delta | \epsilon_{\mathrm{XC}}^{\sigma} | \mu \rangle^{(n-1)}. \tag{45}$$

The first term is concerned to the AO's only within part I and the second term to those between part I and part II, respectively (AO's μ and ν belong always to part I, and δ and γ to part II). In the aforementioned, the following relations are assumed for the step n $(>n')$,

$$\langle \delta | \nu_{\mathrm{XC}}^{\sigma} | \gamma \rangle_{j_p}^{(n)} \cong \langle \delta | \nu_{\mathrm{XC}}^{\sigma} | \gamma \rangle_{j_p}^{(n-1)}, \quad P_{\delta\gamma}^{(n)} \cong P_{\delta\gamma}^{(n-1)}, \tag{46}$$

$$\langle \delta | \nu_{\mathrm{XC}}^{\sigma} | \mu \rangle_{j_p}^{(n)} \cong \langle \delta | \nu_{\mathrm{XC}}^{\sigma} | \mu \rangle_{j_p}^{(n-1)}, \quad P_{\delta\mu}^{(n)} \cong P_{\delta\mu}^{(n-1)}. \tag{47}$$

Those assumptions are nearly exact, because the interaction between the AO included in part I and the electron density on the cell J added at step n becomes nearly zero after step n'. As a result, it can be pointed out that the numerical integration method in the XC potential makes it possible to incorporate the contribution from the potential in part I into part II with good accuracy. In other words, nearly exact XC potentials for part II can be obtained only from part II without making electron density on the basis of grid points in part I.

Consequently, the outline of the entire calculation process is summarized by the flow chart in Fig. 2, where N is the number of units required to be contained in the final polymer. In Fig. 2, $\phi_i(A)\{\chi\}$ means that the LMO, which localized on the region A, has the AO basis $\{\chi\}$ over the whole cluster. $\phi_i(A)\{\chi(\mathrm{II})\}$ means that the LMO has the AO basis only in part II. During all steps the LMO's $\phi_i(A)$ are constantly removed in each elongation cycle. Therefore, as far as these LMO's have little influence on the attacking monomer, the electronic states after the diagonalization should give good agreements with those by the conventional direct calculations. The accuracy of the results depends on the localizability of the LMO's and also the distance between the region A of the polymer and the attacking monomer. After step n', that is, after the condition Eq. (18) is satisfied, the AO's and grid points in the inactive region (part I) are additionally removed in the subsequent cycles. In the evaluation of the Coulomb and XC potentials for part II, any approximation other than the relation

$$\rho(r)^{(n)} \cong \rho(r)^{(n-1)} \quad [\text{step } n \ (>n'), r \in \text{part I}] \tag{48}$$

is not introduced. As far as the relation is a good approximation, the results obtained after dropping out the bases (AO's and grid points) should give nearly the same results as those obtained by the elongation method without any dropping out those bases. Thus, we can obtain the electronic structure of a long cluster efficiently and accurately.

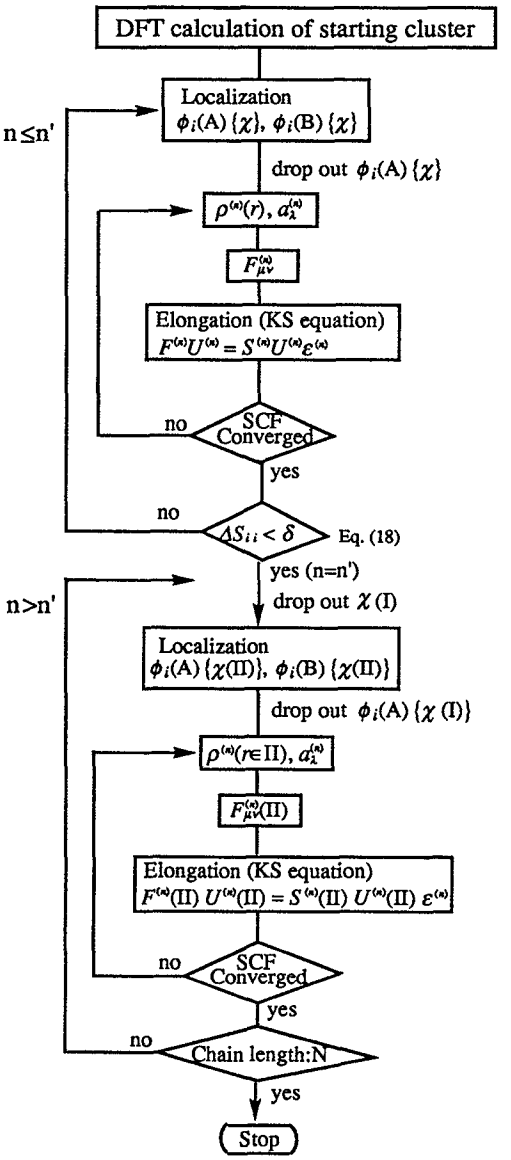

FIG. 2. Flow chart for the procedure of localization and elongation.

III. RESULTS AND DISCUSSION

To investigate the validity and efficiency of this treatment, we have tested it on a hypothetical polymer system consisting of regularly arranged hydrogen molecules shown in Fig. 3. The distance between the hydrogen molecules was tentatively assumed to be 3.0 Å and the distance between the two hydrogen atoms in the molecule was 0.74 Å. Four GTO's for the $1s$ orbital and 1 GTO for the $2s$ orbital, (41), were used as the basis set for the hydrogen atom. The

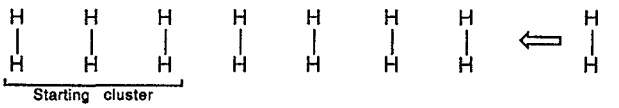

FIG. 3. The hypothetical polymer system consisting of regularly arranged hydrogen molecules. The intermolecular distances are fixed as 3.0 Å and the bond distances as 0.74 Å.

TABLE I. Total energy comparison of parallely arranged hydrogen molecule cluster $(3+n)H_2$.

		Direct LSD[a]			Elongation (N_s=3)[b]		
n	Cluster	Total energy (a.u)	CPU[c] (min.)	Space[d] (MB)	Total energy (a.u)	CPU (min.)	Space (MB)
	H_2	−1.118 876					
	$3H_2$	−3.355 809					
1	$4H_2$	−4.474 319	0.33	130	−4.474 319 (0.000 000)[e]	0.18	130
2	$5H_2$	−5.592 830	0.48	252	−5.592 830 (0.000 000)	0.25	252
5	$8H_2$	−8.948 362	0.92	1,014	−8.948 362 (0.000 000)	0.53	780
7	$10H_2$	−11.185 383	1.52	1,968	−11.185 383 (0.000 000)	0.82	974
12	$15H_2$	−16.777 937	4.95	6,588	−16.777 937 (0.000 000)	0.96	1462
17	$20H_2$	−22.370 491	11.12	15,552	−22.370 490 (0.000 001)	1.26	1,949
22	$25H_2$	−27.963 045	25.68	30,300	−27.963 043 (0.000 002)	1.80	2,436
27	$30H_2$	−33.555 599	36.49	52,272	−33.555 596 (0.000 003)	2.39	2,923
32	$35H_2$	−39.148 153	64.27	82,908	−39.148 151 (0.000 002)	3.28	3,410
37	$40H_2$	−44.740 706	95.21	123,648	−44.740 704 (0.000 002)	4.37	3,898
42	$45H_2$	−50.333 260	134.15	175,932	−50.333 258 (0.000 002)	5.42	4,385
47	$50H_2$	−55.925 814	181.35	241,200	−55.925 811 (0.000 003)	6.83	4,872

[a]Conventional LSD calculations by using the DeMon program package.
[b]Elongation calculations by taking $3H_2$ as the starting cluster.
[c]CPU time on Convex 220.
[d]Disk space required for the storage of two-electron integrals.
[e]Elongation-direct LSD.

cluster with $3H_2$ was calculated initially, the CMO's thus obtained were localized into the first H_2 molecule (A region) and into the other $2H_2$ molecules (B region), and then four orbitals that were already localized on the region A (one is the occupied orbital and the other three are the vacant ones) were removed. Thus, we diminished the dimension of the matrix for the cluster by 4. At the same time, however, we added four orbitals, the one occupied and the three vacant CMO's of the attacking hydrogen molecule. As a whole, the dimension of the diagonalization by Eq. (8) remained constant even after the cluster was elongated by one hydrogen molecule. The repetition of this procedure has made it possible to calculate the electronic structure of the cluster with nearly infinite length with the constant dimension of the eigenvalue problem, that is, the dimension 12 (=4×3) which was equal to that of the starting cluster. After elongation with the fourth H_2 molecules (n'=4 in Fig. 1), it was found that the coefficients of the AO's in the remotest hydrogen molecule moiety became negligibly small in the MO's employed [the contribution of this part, Eq. (18), is less than 10^{-8}] and, hence, the AO's in the remotest hydrogen molecule were dropped thereafter. Accordingly, the number of AO's in all LMO's also remained to be constant 4×7, corresponding to the dimension of part II.

In the evaluation of the XC potentials, the grid points in the part I were also omitted after fourth cycle (n'=4 in Fig. 1). For the test calculation, coarse grids were used around each hydrogen atom within local density approximation (LDA).[12,13] For the fitting of the CD potential, five auxiliary functions as the s type and ten functions as the spd type were located for every hydrogen atom.

To prove the validity of the present method, the usual calculations (direct LSD) by the DeMon program package were performed on the whole cluster for comparison. In Table I, the total energies by the present elongation method are listed for various lengths of the clusters along with those by the usual LSD method. The good agreements are obtained between the both treatments and any error does not arise even after removing the AO's and grid points in part I (at n=5 in this calculation). Besides, the elongation method saves much computational time in comparison with the direct LSD method, and this advantage increases efficiently with the length of the clusters. However, the CPU time for the elongation method also increases gradually because of the increasing in both of the auxiliary functions and the second term of Eq. (35). The disk space required for the storage of the two-electron integrals is proportional to the number of the auxiliary functions $\sim M$ in the present method, which is greatly reduced rather than that by the direct LSD calculations proportional to N^2M. Those results for the simple

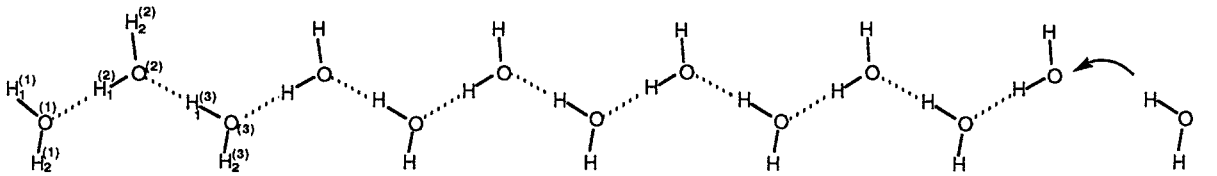

FIG. 4. Model clusters of water molecules. The geometries used here are $\angle$COH=113.26°, $\angle$HO···H=124.98°, $d_{O\text{-}H}$=0.9499 Å, $d_{O\cdots H}$=1.6954 Å, and $d_{O\cdots O}$=2.6727 Å.

model system suggest applicability of our treatment to real systems.

Next, we have applied our treatment to the one-dimensional water clusters shown in Fig. 4. The geometry was adopted which has been optimized by the *ab initio* calculations including MP2 correlation correction under periodic boundary condition. The 4-31G basis set and medium grids were used for all atoms. In the XC potential, the nonlocal corrections were included using Becke's exchange[14] and Perdew's correlation.[15] To investigate the N_s (the cell number of the starting cluster) dependencies on the accuracy and efficiency of our treatment, various N_s are adopted for the cluster elongations. The total energies and CPU times are listed for each step in Table II in comparison with those by the direct LSD calculations.

In the case of N_s=3, the starting cluster 3(H_2O) is calculated before the elongation, the CMO's thus obtained were localized into the first H_2O molecule (*A* region) and into the other $2H_2O$ (*B* region), and thereafter H_2O monomer was added one by one. As a whole, the dimension of the diagonalization remained constant to be 13×3 and after n=4 the AO's in region *A* are removed in every cycle. In the subsequent cycles the number of AO's became constant to be 13×7 and the grid points were also generated only on the $7H_2O$ near the attacking monomer. From Table II it can be seen that the differences between the elongation and direct LSD methods are accumulated by about 0.04 kcal/mol at every step. The errors come from the small size of the starting cluster, because the LMO's localized in region *A* are removed at every step, although the interaction between those LMO's and the attacking monomer still remains. Even after step 4, where the AO's and grid points in the terminal region are initially removed, additional errors do not arise. However, at $20H_2O$ (n=17) the difference between the elongation method and direct LSD is summarized up to 0.68 kcal/mol. This means that the larger starting cluster is required for getting the more accurate results. The CPU times by the elongation method are much more advantageous in comparison to those by the direct LSD method.

In the case of N_s=4, the starting cluster 4(H_2O) is calculated before the elongation, the CMO's thus obtained were localized into the first H_2O molecule (*A* region) and into the other $3H_2O$ (*B* region), and thereafter the H_2O monomer is added one by one as well as the case of N_s=3. As a whole, the dimension of the diagonalization remained constant to be 13×4 and after n=5 the AO's in region *A* are removed in every cycle. In subsequent cycles the number of AO's became constant to be 13×9 and the grid points were also generated only on the $9H_2O$ near the attacking monomer. The differences between the elongation and direct LSD methods are accumulated by about 0.009 kcal/mol at every step, which is greatly improved compared to the cases of the N_s=3. Even at $20H_2O$ (n=16), the agreement between the two methods are very good within thermal energy. This implies that if N_s=4 is used as the starting cluster, the interaction between the LMO's localized on region *A* and the attacking monomer becomes negligibly small.

In the case of N_s=5, the starting cluster 5(H_2O) is calculated before the elongation, the CMO's thus obtained were localized into the first H_2O molecule (*A* region) and into the other $4H_2O$ (*B* region). The dimension of the diagonalization remained constant to be 13×5 and after n=6 the AO's in region *A* were removed in every cycle. In subsequent cycles the number of AO's became constant to be 13×11 and the grid points were also generated only on the $11H_2O$ near the attacking monomer. The differences between the two methods are accumulated by about 0.004 kcal/mol at every step, which is further improved compared to the case of the N_s=4. Even at $20H_2O$ (n=16), the total energies are in excellent agreement between the two methods. However, the CPU time required for the elongation increases with the size of the N_s because of the increasing AO's, MO's, and grid points employed. Therefore, the starting cluster should be selected at the balance between the accuracy desired and the CPU time required.

In order to investigate the individual contribution in the total energies, we divide those into the core Hamiltonian (E_{core}) (kinetic energy+electron-nuclear attraction energy), electron–electron Coulomb repulsion (E_{Colomb}), exchange (E_{ex}), and correlation (E_{corr}) energies. The values obtained by the elongation method are listed in Table III. In Table III the values for 6–12H_2O are given by the elongation method (N_s=5), and those for 2–5H_2O are supplied by the direct LSD calculations because the results for these small clusters can not be provided by the elongation method using N_s=5 as the staring. As predicted, the core and Coulomb energies are greatly increased in the process of the cluster elongation and those increments in each step do not converge until $20H_2O$. On the other hand, the increments in the exchange and correlation contributions are rapidly converged rather than the other terms which come from strong Coulomb interactions. After $12H_2O$ for the correlation energy and after $10H_2O$ for the exchange energy, the constant contributions are successively added by the interaction with an attacking molecule.

TABLE II. Total energy comparison of water clusters by the 4-31G basis set and the Becke–Perdew potential.

	Direct LSD		Elongation					
			$N_s=3$		$N_s=4$		$N_s=5$	
	Total energy (a.u)	CPU (min.)	Total energy (a.u)	CPU (min.)	Total energy (a.u)	CPU (min.)	Total energy (a.u)	CPU (min.)
H_2O	−76.323 854							
$2H_2O$	−152.662 961							
$3H_2O$	−229.008 329							
$4H_2O$	−305.355 682	8.65	−305.355 654 (0.000 028)	7.20				
$5H_2O$	−381.703 821	15.53	−381.703 747 (0.000 074)	12.49	−381.703 817 (0.000 004)	12.63		
$6H_2O$	−458.052 362	28.20	−458.052 233 (0.000 129)	19.20	−458.052 350 (0.000 012)	20.05	−458.052 361 (0.000 001)	20.17
$7H_2O$	−534.401 118	42.25	−534.400 928 (0.000 190)	27.54	−534.401 094 (0.000 024)	28.42	−534.401 114 (0.000 004)	30.49
$8H_2O$	−610.750 007	56.55	−610.749 754 (0.000 253)	29.71	−610.749 970 (0.000 037)	42.61	−610.749 999 (0.000 008)	42.54
$9H_2O$	−687.098 980	74.75	−687.098 661 (0.000 319)	31.47	−687.098 929 (0.000 051)	53.17	−687.098 967 (0.000 013)	56.76
$10H_2O$	−763.448 012	111.23	−763.447 626 (0.000 386)	33.49	−763.447 946 (0.000 066)	56.64	−763.447 994 (0.000 018)	74.92
$11H_2O$	−839.797 084	133.12	−839.796 631 (0.000 453)	35.38	−839.797 003 (0.000 081)	60.06	−839.797 060 (0.000 024)	95.10
$12H_2O$	−916.146 187	187.58	−916.145 666 (0.000 521)	37.12	−916.146 091 (0.000 098)	62.91	−916.146 157 (0.000 030)	96.52
$13H_2O$	−992.495 313	247.35	−992.494 722 (0.000 591)	39.18	−992.495 201 (0.000 112)	65.04	−992.495 277 (0.000 036)	98.24
$14H_2O$	−1068.844 457	246.63	−1068.843 797 (0.000 660)	41.46	−1068.844 329 (0.000 128)	67.65	−1068.844 415 (0.000 042)	99.88
$15H_2O$	−1145.193 615	302.43	−1145.192 886 (0.000 729)	43.44	−1145.193 471 (0.000 144)	70.59	−1145.193 566 (0.000 049)	110.59
$16H_2O$	−1221.542 784	410.20	−1221.541 985 (0.000 799)	45.73	−1221.542 623 (0.000 161)	73.53	−1221.542 728 (0.000 056)	108.82
$17H_2O$	−1297.891 963	467.38	−1297.891 094 (0.000 869)	47.16	−1297.891 785 (0.000 178)	75.99	−1297.891 900 (0.000 063)	117.04
$18H_2O$	−1374.241 149	813.47	−1374.240 210 (0.000 939)	49.60	−1374.240 955 (0.000 194)	79.27	−1374.241 079 (0.000 070)	118.08
$19H_2O$	−1450.590 342	920.18	−1450.589 331 (0.001 011)	52.68	−1450.590 131 (0.000 211)	83.37	−1450.590 265 (0.000 077)	121.84
$20H_2O$	−1526.939 540	1063.68	−1526.938 459 (0.001 081)	56.98	−1526.939 312 (0.000 228)	86.28	−1526.939 456 (0.000 084)	120.31

In Table IV, the interaction energies between the cluster and the attacking molecule are listed for various N_s in comparison with those by the direct calculations. The interaction energy is given by the difference between the total energy of the cluster elongated and the sum of the total energies of the cluster in the previous step and the attacking monomer. The values by the elongation method are in excellent agreement with those obtained by the direct LSD method over all steps. The agreements between them become better with increasing N_s. The absolute values of the interaction energies become larger as the chain length increases. In Table IV the exchange (ΔE_{ex}^{int}) and correlation (ΔE_{corr}^{int}) contributions to the interaction energies are also listed together. These contributions are not responsible for the interaction energy. This implies that the other contributions which come from electrostatic interaction dominate the interaction energy. The correlation energy which has less contribution rather than the exchange energy in the total energy (as seen in Table III) is more responsible for the interaction energy. The correlation contributions become somewhat more rapidly constant than the exchange contributions. For such regular systems, new information will not be provided any more for the further extension of the cluster. During all steps the absolute values of the interaction energies are too large compared with experimental data, because small basis set like 4-31G provides a large dipole moment as shown later, which leads to the overestimating in electrostatic interaction and, hence, gives rise to the large interaction energy. Those values are greatly improved by including diffuse and polarization functions in the basis set as well as those basis set super position error (BSSE). However, we will not discuss the reliability of the absolute values, because our purpose of the present work is to develop the elongation method and compare the results with those by the conventional treatment.

In Table V, the atomic populations are listed for the comparison between the elongation ($N_s=3$–5) and the direct LSD methods. The electron density has a slight tendency to be transferred from the first terminal into the end terminal.

TABLE III. The core, Coulomb, exchange, and correlation contributions (in a.u.) in the total energies of water clusters and those increments by the elongation indicated in parentheses.

Cluster	$h^{(n)}$	U_C	U_{ex}	U_{corr}
$2H_2O$	−285.819 852	113.791 343	−18.061 536	−0.744 328
	(−162.644 392)	(66.781 771)	(−9.026 898)	(−0.374 965)
$3H_2O$	−470.803 469	191.737 172	−27.087 739	−1.119 445
	(−184.983 617)	(77.945 829)	(−9.026 203)	(−0.375 117)
$4H_2O$	−670.427 339	277.003 122	−36.113 189	−1.494 535
	(−199.623 870)	(85.265 950)	(−9.025 450)	(−0.375 090)
$5H_2O$	−881.213 192	367.848 063	−45.138 260	−1.869 611
	(−210.785 853)	(90.844 941)	(−9.025 071)	(−0.375 076)
$6H_2O$	−1100.872 956	463.129 079	−54.163 151	−2.244 672
	(−219.659 764)	(95.281 016)	(−9.024 891)	(−0.375 061)
$7H_2O$	−1327.974 094	562.130 327	−63.187 975	−2.619 732
	(−227.101 138)	(99.001 248)	(−9.024 824)	(−0.375 060)
$8H_2O$	−1561.434 046	664.311 246	−72.212 774	−2.994 791
	(−233.459 952)	(102.180 919)	(−9.024 799)	(−0.375 059)
$9H_2O$	−1800.475 189	769.282 701	−81.237 552	−3.369 850
	(−239.041 143)	(104.971 455)	(−9.024 778)	(−0.375 059)
$10H_2O$	−2044.468 071	876.730 201	−90.262 322	−3.744 908
	(−243.992 882)	(107.447 500)	(−9.024 770)	(−0.375 058)
$11H_2O$	−2292.925 852	986.410 143	−99.287 082	−4.119 967
	(−248.457 781)	(109.679 942)	(−9.024 760)	(−0.375 059)
$12H_2O$	−2545.437 507	1098.117 131	−108.311 838	−4.495 026
	(−252.511 655)	(111.706 988)	(−9.024 756)	(−0.375 059)
$13H_2O$	−2801.669 864	1211.684 470	−117.336 588	−4.870 085
	(−256.232 357)	(113.567 339)	(−9.024 750)	(−0.375 059)
$14H_2O$	−3061.333 612	1326.967 575	−126.361 338	−5.245 144
	(−259.663 748)	(115.283 105)	(−9.024 750)	(−0.375 059)
$15H_2O$	−3324.186 506	1443.845 254	−135.386 084	−5.620 203
	(−262.852 894)	(116.877 679)	(−9.024 746)	(−0.375 059)
$16H_2O$	−3590.013 917	1562.210 239	−144.410 828	−5.995 261
	(−265.827 411)	(118.364 985)	(−9.024 744)	(−0.375 058)
$17H_2O$	−3858.631 812	1681.970 467	−153.435 571	−6.370 320
	(−268.617 895)	(119.760 228)	(−9.024 743)	(−0.375 059)
$18H_2O$	−4129.874 661	1803.043 205	−162.460 314	−6.745 379
	(−271.242 849)	(121.072 738)	(−9.024 743)	(−0.375 059)
$19H_2O$	−4403.597 930	1925.356 154	−171.485 054	−7.120 438
	(−273.723 269)	(122.312 949)	(−9.024 740)	(−0.375 059)
$20H_2O$	−4679.670 081	2048.843 567	−180.509 795	−7.495 497
	(−276.072 151)	(123.487 413)	(−9.024 741)	(−0.375 059)

The agreement between the both methods becomes better with increasing N_s. However, in the first terminal (about until fifth units), the agreement is insufficient. The electron density that is provided from the LMO's removed already at the beginning of the elongation becomes unaffected by the further elongation and therefore generates some slight errors in subsequent cycles. Those disagreements between the two methods can be removed by using a longer cluster in the starting of the elongation. On the other hand, in the reactant end terminal, the agreements between the two methods are excellent. This implies that the interaction between the cluster and attacking monomer is exactly evaluated in our scheme and the local band structures in its neighborhood are adequately provided with good accuracy in the process of the cluster elongation.

In Table VI, overlap populations between hydrogen-bonding atoms are listed for the both methods. All the hydrogen-bonding indicate a covalent nature, which is somewhat reduced on the both of the first and the end terminals. As is the case of the atomic populations, the agreement between the both methods becomes better with increasing N_s and it becomes excellent in the reactant end terminal.

Dipole moments are listed in the Table VII with those increments by the cluster extension in parentheses. Those values are overall too large in comparison with the experimental data because of the small basis set. As mentioned previously, those large dipole moments cause the overestimating in electrostatic interaction, which leads to the large interaction energy between water molecules. The agreement between the direct LSD and the elongation method is not sufficient even with $N_s=5$, but it becomes better with increasing N_s. As seen in Table V, the electron densities in the first terminal region, which are in slight disagreement between the two methods, give rise to some errors in the dipole moments. However, the values obtained by the elongation method using $N_s=5$ seem to be adequately useful in the investigation of one-electron natures. The increment in the dipole moments increases as the cluster grows, and it becomes almost constant after about $10H_2O$, although there is a slight difference between the odd-number and ever-number clusters. Those tendencies, characteristic features in

TABLE IV. Interaction energies (kcal/mol) of water clusters.

	ΔE^{int}					
		Elongation				
Cluster	Direct LSD	$N_s=3$	$N_s=4$	$N_s=5$	$\Delta E_{ex}^{int\ a}$	$\Delta E_{corr}^{int\ b}$
$2H_2O$	−10.02				−3.15	−3.90
$3H_2O$	−13.50				−2.71	−4.00
$4H_2O$	−14.75	−14.73			−2.24	−3.98
$5H_2O$	−15.24	−15.21	−15.24		−2.00	−3.97
$6H_2O$	−15.49	−15.46	−15.48	−15.49	−1.89	−3.97
$7H_2O$	−15.63	−15.59	−15.62	−15.62	−1.84	−3.96
$8H_2O$	−15.71	−15.67	−15.70	−15.71	−1.83	−3.96
$9H_2O$	−15.76	−15.72	−15.75	−15.76	−1.82	−3.96
$10H_2O$	−15.80	−15.76	−15.79	−15.80	−1.81	−3.96
$11H_2O$	−15.82	−15.78	−15.82	−15.82	−1.80	−3.96
$12H_2O$	−15.84	−15.80	−15.83	−15.84	−1.80	−3.96
$13H_2O$	−15.86	−15.81	−15.85	−15.85	−1.80	−3.96
$14H_2O$	−15.87	−15.83	−15.86	−15.87	−1.80	−3.96
$15H_2O$	−15.88	−15.84	−15.87	−15.87	−1.80	−3.96
$16H_2O$	−15.89	−15.84	−15.87	−15.88	−1.79	−3.96
$17H_2O$	−15.89	−15.85	−15.88	−15.89	−1.79	−3.96
$18H_2O$	−15.90	−15.85	−15.89	−15.89	−1.79	−3.96
$19H_2O$	−15.90	−15.86	−15.89	−15.90	−1.79	−3.96
$20H_2O$	−15.90	−15.86	−15.89	−15.90	−1.79	−3.96

[a]The exchange contribution in the interaction energy.
[b]The correlation contribution in the interaction energy.

hydrogen-bonding systems, are well described even by using the small N_s.

At last, we applied this method to the hydrogen-bonding system of formamides with the two models, translational motif and screw axis motif. This is a simple model for the hydrogen-bonding system in polypeptide. The former is defined as model 1 and the latter as model 2 as shown in Fig. 5. As is the case of water clusters, the 4-31G basis set and medium grids were used for all atoms. In the XC potential, the nonlocal corrections were included using Becke's

TABLE V. Atomic populations of the water cluster $20H_2O$. The numbering of the atoms is shown in Fig. 4.

	$O^{(1)}$	$H_1^{(1)}$	$H_2^{(1)}$	$O^{(2)}$	$H_1^{(2)}$	$H_2^{(2)}$	$O^{(3)}$	$H_1^{(3)}$	$H_2^{(3)}$	$O^{(4)}$	$H_1^{(4)}$	$H_2^{(4)}$	$O^{(5)}$	$H_1^{(5)}$	$H_2^{(5)}$
Elongation															
$N_s=3$	8.5857	0.6716	0.6458	8.6422	0.6726	0.6712	8.6446	0.6749	0.6778	8.6461	0.6749	0.6782	8.6484	0.6715	0.6787
$N_s=4$	8.5870	0.6690	0.6442	8.6437	0.6725	0.6698	8.6483	0.6717	0.6764	8.6498	0.6717	0.6769	8.6502	0.6716	0.6775
$N_s=5$	8.5877	0.6678	0.6437	8.6442	0.6721	0.6694	8.6488	0.6716	0.6761	8.6503	0.6715	0.6766	8.6507	0.6715	0.6772
Direct LSD	8.5887	0.6662	0.6431	8.6450	0.6716	0.6689	8.6495	0.6713	0.6756	8.6510	0.6713	0.6761	8.6514	0.6713	0.6767
	$O^{(6)}$	$H_1^{(6)}$	$H_2^{(6)}$	$O^{(7)}$	$H_1^{(7)}$	$H_2^{(7)}$	$O^{(8)}$	$H_1^{(8)}$	$H_2^{(8)}$	$O^{(9)}$	$H_1^{(9)}$	$H_2^{(9)}$	$O^{(10)}$	$H_1^{(10)}$	$H_2^{(10)}$
Elongation															
$N_s=3$	8.6473	0.6743	0.6788	8.6489	0.6715	0.6788	8.6475	0.6740	0.6790	8.6490	0.6715	0.6789	8.6476	0.6739	0.6790
$N_s=4$	8.6506	0.6715	0.6775	8.6507	0.6715	0.6777	8.6508	0.6715	0.6776	8.6508	0.6714	0.6777	8.6508	0.6714	0.6777
$N_s=5$	8.6510	0.6614	0.6772	8.6511	0.6714	0.6773	8.6512	0.6713	0.6773	8.6513	0.6713	0.6773	8.6513	0.6713	0.6773
Direct LSD	8.6517	0.6712	0.6767	8.6518	0.6712	0.6769	8.6519	0.6712	0.6769	8.6519	0.6711	0.6769	8.6519	0.6712	0.6769
	$O^{(11)}$	$H_1^{(11)}$	$H_2^{(11)}$	$O^{(12)}$	$H_1^{(12)}$	$H_2^{(12)}$	$O^{(13)}$	$H_1^{(13)}$	$H_2^{(13)}$	$O^{(14)}$	$H_1^{(14)}$	$H_2^{(14)}$	$O^{(15)}$	$H_1^{(15)}$	$H_2^{(15)}$
Elongation															
$N_s=3$	8.6491	0.6714	0.6789	8.6477	0.6739	0.6790	8.6491	0.6714	0.6789	8.6477	0.6739	0.6790	8.6491	0.6714	0.6789
$N_s=4$	8.6509	0.6714	0.6777	8.6509	0.6714	0.6777	8.6509	0.6714	0.6777	8.6509	0.6714	0.6777	8.6509	0.6714	0.6777
$N_s=5$	8.6513	0.6713	0.6773	8.6514	0.6713	0.6773	8.6514	0.6713	0.6774	8.6514	0.6713	0.6773	8.6514	0.6713	0.6773
Direct LSD	8.6519	0.6712	0.6770	8.6519	0.6712	0.6770	8.6518	0.6712	0.6770	8.6518	0.6713	0.6771	8.6517	0.6714	0.6772
	$O^{(16)}$	$H_1^{(16)}$	$H_2^{(16)}$	$O^{(17)}$	$H_1^{(17)}$	$H_2^{(17)}$	$O^{(18)}$	$H_1^{(18)}$	$H_2^{(18)}$	$O^{(19)}$	$H_1^{(19)}$	$H_2^{(19)}$	$O^{(20)}$	$H_1^{(20)}$	$H_2^{(20)}$
Elongation															
$N_s=3$	8.6477	0.6739	0.6790	8.6492	0.6714	0.6789	8.6472	0.6784	0.6847	8.6472	0.6784	0.6847	8.6925	0.6990	0.7153
$N_s=4$	8.6509	0.6714	0.6777	8.6508	0.6713	0.6777	8.6498	0.6734	0.6795	8.6478	0.6782	0.6849	8.6927	0.6993	0.7154
$N_s=5$	8.6513	0.6712	0.6773	8.6509	0.6722	0.6779	8.6498	0.6734	0.6795	8.6478	0.6782	0.6849	8.6927	0.6993	0.7154
Direct LSD	8.6514	0.6717	0.6775	8.6510	0.6722	0.6779	8.6498	0.6735	0.6795	8.6478	0.6782	0.6849	8.6927	0.6993	0.7154

TABLE VI. Overlap populations between hydrogen-bonding atoms of the water cluster $20H_2O$.

	$O^{(1)}$–$H_1^{(2)}$	$O^{(2)}$–$H_1^{(3)}$	$O^{(3)}$–$H_1^{(4)}$	$O^{(4)}$–$H_1^{(5)}$	$O^{(5)}$–$H_1^{(6)}$
Elongation					
N_s=3	0.1634	0.1820	0.1871	0.1894	0.1903
N_s=4	0.1670	0.1861	0.1913	0.1936	0.1946
N_s=5	0.1683	0.1876	0.1929	0.1952	0.1961
Direct LSD	0.1700	0.1896	0.1949	0.1972	0.1982
	$O^{(6)}$–$H_1^{(7)}$	$O^{(7)}$–$H_1^{(8)}$	$O^{(8)}$–$H_1^{(8)}$	$O^{(9)}$–$H_1^{(10)}$	$O^{(10)}$–$H_1^{(11)}$
Elongation					
N_s=3	0.1908	0.1911	0.1913	0.1914	0.1915
N_s=4	0.1951	0.1954	0.1956	0.1957	0.1958
N_s=5	0.1967	0.1970	0.1972	0.1973	0.1974
Direct LSD	0.1987	0.1990	0.1991	0.1992	0.1992
	$O^{(11)}$–$H_1^{(12)}$	$O^{(12)}$–$H_1^{(13)}$	$O^{(13)}$–$H_1^{(14)}$	$O^{(14)}$–$H_1^{(15)}$	$O^{(15)}$–$H_1^{(16)}$
Elongation					
N_s=3	0.1916	0.1916	0.1917	0.1917	0.1917
N_s=4	0.1959	0.1959	0.1960	0.1960	0.1960
N_s=5	0.1975	0.1975	0.1976	0.1976	0.1976
Direct LSD	0.1992	0.1992	0.1990	0.1988	0.1984
	$O^{(16)}$–$H_1^{(17)}$	$O^{(17)}$–$H_1^{(18)}$	$O^{(18)}$–$H_1^{(19)}$	$O^{(19)}$–$H_1^{(20)}$	
Elongation					
N_s=3	0.1917	0.1918	0.1902	0.1724	
N_s=4	0.1960	0.1956	0.1906	0.1726	
N_s=5	0.1974	0.1958	0.1907	0.1726	
Direct LSD	0.1975	0.1958	0.1907	0.1726	

exchange[14] and Perdew's correlation.[15] The results obtained by the present method are written in Table VIII for model 1. In Table VIII, the total energies and interaction energies are listed with those exchange and correlation components for each elongation step. The increments in total energies (in parentheses) show that the electronic properties are adequately converged within ten clusters. Although the correlation contributions are very small compared to the exchange contributions in the total energies, both contributions become comparable in the interaction energies. Dipole moments are also listed in the most right-hand side. Those increments increase with the cluster size, but they become almost constant after 5 units. Listed in Table IX are the energetic behavior and dipole moments for the model 2. The total energies of

TABLE VII. Dipole moments (a.u.) of water clusters and those increments in parentheses.

		Elongation		
Cluster	Direct LSD	N_s=3	N_s=4	N_s=5
H_2O	0.872			
$2H_2O$	1.844(0.972)			
$3H_2O$	3.032(1.188)			
$4H_2O$	4.198(1.166)	4.182		
$5H_2O$	5.409(1.211)	5.373(1.191)	5.403	
$6H_2O$	6.602(1.193)	6.543(1.170)	6.587(1.184)	6.598
$7H_2O$	7.817(1.215)	7.735(1.210)	7.793(1.206)	7.810(1.212)
$8H_2O$	9.018(1.201)	8.912(1.177)	8.983(1.190)	9.006(1.196)
$9H_2O$	10.235(1.217)	10.103(1.191)	10.189(1.206)	10.217(1.211)
$10H_2O$	11.440(1.205)	11.283(1.180)	11.382(1.193)	11.416(1.199)
$11H_2O$	12.656(1.216)	12.474(1.191)	12.587(1.205)	12.626(1.210)
$12H_2O$	13.864(1.208)	13.655(1.181)	13.783(1.196)	13.827(1.201)
$13H_2O$	15.080(1.216)	14.846(1.191)	14.987(1.204)	15.037(1.210)
$14H_2O$	16.289(1.209)	16.028(1.182)	16.184(1.197)	16.239(1.202)
$15H_2O$	17.505(1.216)	17.219(1.191)	17.388(1.204)	17.449(1.210)
$16H_2O$	18.715(1.210)	18.402(1.183)	18.586(1.198)	18.652(1.203)
$17H_2O$	19.931(1.216)	19.592(1.190)	19.790(1.204)	19.861(1.209)
$18H_2O$	21.142(1.211)	20.776(1.184)	20.988(1.198)	21.065(1.204)
$19H_2O$	22.358(1.216)	21.966(1.190)	22.191(1.204)	22.274(1.209)
$20H_2O$	23.569(1.211)	23.150(1.184)	23.390(1.199)	23.478(1.204)

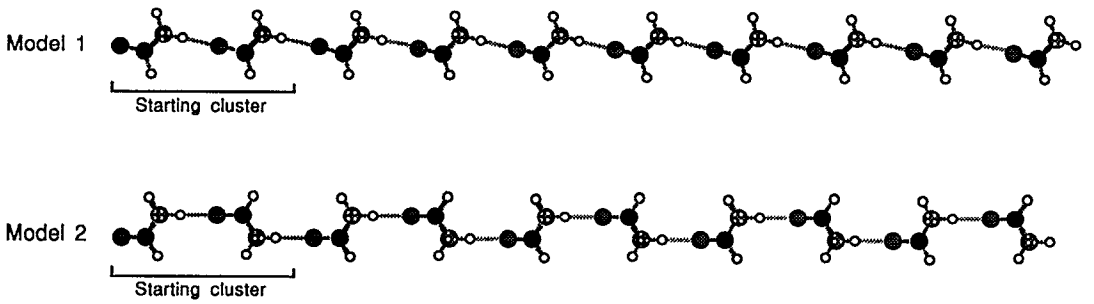

FIG. 5. Model clusters of formamide molecules. Open circe, solid circle, meshed circule, and cross-hatched circle indicate hydrogen, carbon, nitrogen, and oxygen atoms, respectively. All of bond angles are fixed as 120°. The bond lengths are d_{N-O}=2.88 Å, d_{C-N}=1.30 Å, $d_{C=O}$=1.255 Å, d_{N-H}=1.002 Å, and d_{C-H}=1.098 Å.

model 2 are only slight more stable than those of model 1, but energetic behaviors are very similar between the both models. Although the dipole moments tend to be somewhat enhanced in the odd numbered units, they are expected to become constant in the increments after ten units.

Atomic population on each atom, net charge on each unit and overlap population on the hydrogen-bonding H···O are listed in Table X for the both models. For comparison, net charge and overlap population of $10H_2O$, which are obtained by the elongation method, are also listed in the lower right-hand side. The results for the both models of $10(CHONH_2)$ are very similar with each other. In both cases, the net charge on each unit tends to be assembled on the left-hand side of the cluster and thus only the final unit shows a positive charge. On the other hand, in $10H_2O$ the electron density is transferred from the left-hand side to the right-hand side, reactant end part. Overlap populations on the hydrogen bonding H···O in model 1 are very close to those of model 2. They indicate a covalent nature which becomes somewhat larger with the unit number, in contrast to the case of $10H_2O$ which shows an end effect. However, for a more detail discussion, including diffuse and polarization functions will be inevitable.

The results by the direct LSD method cannot be shown, because convergent results could not be provided for longer clusters than 4 units of the formamides by the DeMon program package. However, the results obtained by the elongation method would be reliable with good accuracy, since the

TABLE VIII. Energetic behavior and dipole moment of model 1 and those increments in parentheses by the 4-31G basis set and the Becke–Perdew potential.

Cluster	Total energy[a] (a.u.)	U_{ex}[b] (a.u.)	U_{corr}[c] (a.u.)	E^{int}[d]	E_{ex}^{int}[e]	E_{corr}^{int}[f]	Dipole moment (a.u.)
				(kcal/mol)			
$2CHONH_2$	−339.352 058	−42.355 785	−1.778 907	−10.73	−3.21	−2.28	4.163
	(−169.684 575)	(−21.180 452)	(−0.891 270)				(2.414)
$3CHONH_2$	−509.040 512	−63.536 881	−2.670 195	−13.16	−3.62	−2.28	6.616
	(−169.688 454)	(−21.181 096)	(−0.891 288)				(2.453)
$4CHONH_2$	−678.730 006	−84.718 048	−3.561 484	−13.81	−3.66	−2.29	9.081
	(−169.689 494)	(−21.181 165)	(−0.891 289)				(2.465)
$5CHONH_2$	−848.419 900	−105.899 239	−4.452 773	−14.06	−3.68	−2.29	11.552
	(−169.689 894)	(−21.181 191)	(−0.891 293)				(2.471)
$6CHONH_2$	−1018.109 967	−127.080 464	−5.344 066	−14.17	−3.70	−2.29	14.025
	(−169.690 067)	(−21.181 225)	(−0.891 293)				(2.473)
$7CHONH_2$	−1187.800 134	−148.261 701	−6.235 360	−14.23	−3.70	−2.29	16.499
	(−169.690 167)	(−21.181 237)	(−0.891 293)				(2.474)
$8CHONH_2$	−1357.490 370	−169.442 931	−7.126 653	−14.28	−3.70	−2.29	18.974
	(−169.690 236)	(−21.181 230)	(−0.891 293)				(2.475)
$9CHONH_2$	−1527.180 635	−190.624 181	−8.017 949	−14.30	−3.71	−2.30	21.450
	(−169.690 265)	(−21.181 250)	(−0.891 296)				(2.476)
$10CHONH_2$	−1696.870 926	−211.805 434	−8.909 245	−14.31	−3.71	−2.30	23.926
	(−169.690 291)	(−21.181 253)	(−0.891 296)				(2.476)

[a]Total energy obtained by the Elongation method.
[b]Exchange contribution in the total energy.
[c]Correlation contribution in the total energy.
[d]Interaction energy by the Elongation method.
[e]Exchange contribution in the interaction energy.
[f]Correlation contribution in the interaction energy.

TABLE IX. Energetic behavior and dipole moment of model 2 and those increments in parentheses by the 4-31G basis set and the Becke–Perdew potential.

Cluster	Total energy (a.u.)	U_{ex} (a.u.)	U_{corr} (a.u.)	E^{int} (kcal/mol)	E^{int}_{ex} (kcal/mol)	E^{int}_{corr} (kcal/mol)	Dipole moment (a.u.)
$2CHONH_2$	−339.352 441	−42.355 225	−1.778 886	−10.97	−2.86	−2.27	3.865
	(−169.684 958)	(−21.179 892)	(−0.891 249)				(2.116)
$3CHONH_2$	−509.040 993	−63.535 755	−2.670 143	−13.22	−3.62	−2.27	6.207
	(−169.688 552)	(−21.180 530)	(−0.891 257)				(2.342)
$4CHONH_2$	−678.730 576	−84.716 374	−3.561 402	−13.87	−3.66	−2.27	8.481
	(−169.689 583)	(−21.180 619)	(−0.891 259)				(2.274)
$5CHONH_2$	−848.420 529	−105.897 034	−4.452 663	−14.10	−3.68	−2.28	10.824
	(−169.689 953)	(−21.180 660)	(−0.891 263)				(2.343)
$6CHONH_2$	−1018.110 667	−127.077 718	−5.343 926	−14.22	−3.70	−2.28	13.123
	(−169.690 138)	(−21.180 684)	(−0.891 263)				(2.299)
$7CHONH_2$	−1187.800 899	−148.258 414	−6.235 189	−14.28	−3.70	−2.28	16.462
	(−169.690 232)	(−21.180 696)	(−0.891 263)				(3.339)
$8CHONH_2$	−1357.491 192	−169.439 118	−7.126 454	−14.31	−3.70	−2.28	17.770
	(−169.690 293)	(−21.180 704)	(−0.891 265)				(2.308)
$9CHONH_2$	−1527.181 520	−190.619 828	−8.017 719	−14.34	−3.71	−2.28	20.107
	(−169.690 328)	(−21.180 710)	(−0.891 265)				(2.337)
$10CHONH_2$	−1696.871 877	−211.800 549	−8.908 985	−14.35	−3.71	−2.28	22.420
	(−169.690 357)	(−21.180 721)	(−0.891 266)				(2.313)

difference in total energy between the two methods was about 5.0×10^{-5} a.u. at $n=1$ and the electron densities are also in good agreement between the two methods. This would suggest that our treatment may be more advantage and powerful in treating large molecules and clusters than the direct LSD treatment for the whole system.

IV. CONCLUDING REMARKS

The elongation method has been extended to the level of the density functional theory. In this treatment, the bases on the inactive sites in the elongation step have been removed from the calculations. This treatment has enabled us possible

TABLE X. Atomic population, net charge on each unit, and overlap population on H···O of $10(CHONH_2)$.

Cell number	Model 1 O	C	H	N	H	H	Net charge[a]	H···O[b]	$10H_2O$ (Net charge)[c]	(H···O)[d]
					Model 1					
1	8.5704	5.6358	0.9205	7.5011	0.7457	0.7114	−0.0850	0.1499		
2	8.5890	5.5912	0.8923	7.4917	0.7368	0.7024	−0.0032	0.1560		
3	8.5964	5.5892	0.8887	7.4898	0.7361	0.7006	−0.0008	0.1574		
4	8.5984	5.5889	0.8878	7.4892	0.7360	0.7000	−0.0003	0.1580		
5	8.5992	5.5888	0.8874	7.4890	0.7360	0.6998	−0.0001	0.1582		
6	8.5996	5.5887	0.8873	7.4889	0.7359	0.6997	−0.0000	0.1583		
7	8.5998	5.5887	0.8872	7.4888	0.7359	0.6996	−0.0000	0.1584		
8	8.5999	5.5887	0.8872	7.4888	0.7360	0.6996	−0.0000	0.1584		
9	8.5999	5.5887	0.8871	7.4886	0.7359	0.7010	−0.0013	0.1610		
10	8.5735	5.5750	0.8738	7.4719	0.7119	0.7030	0.0909			
					Model 2					
1	8.5687	5.6356	0.9300	7.4980	0.7418	0.7112	−0.0853	0.1504	(0.1008)	(0.1683)
2	8.5875	5.5915	0.9029	7.4880	0.7310	0.7023	−0.0032	0.1563	(0.0143)	(0.1876)
3	8.5948	5.5894	0.8984	7.4864	0.7315	0.7005	−0.0009	0.1577	(0.0036)	(0.1929)
4	8.5968	5.5890	0.8974	7.4858	0.7315	0.6999	−0.0003	0.1583	(0.0017)	(0.1952)
5	8.5976	5.5888	0.8969	7.4856	0.7316	0.6997	−0.0001	0.1585	(0.0007)	(0.1961)
6	8.5979	5.5888	0.8967	7.4855	0.7316	0.6995	−0.0001	0.1586	(0.0005)	(0.1965)
7	8.5981	5.5888	0.8966	7.4855	0.7317	0.6995	−0.0000	0.1587	(−0.0008)	(0.1951)
8	8.5983	5.5888	0.8965	7.4854	0.7317	0.6994	−0.0000	0.1588	(−0.0026)	(0.1902)
9	8.5983	5.5888	0.8964	7.4853	0.7317	0.7007	−0.0012	0.1612	(−0.0108)	(0.1723)
10	8.5734	5.5750	0.8743	7.4718	0.7114	0.7031	0.0911		(−0.1071)	

[a]Net charge on each unit in $10(CHONH_2)$.
[b]Overlap population on the hydrogen-bonding H···O in $10(CHONH_2)$.
[c]Net charge on each molecule in $10(H_2O)$ for comparison.
[d]Overlap population on the hydrogen bondings in $10(H_2O)$ for comparison.

to treat large clusters within small number of the grid points and two-electron integrals. This method has been applied to regular hydrogen molecule polymers as a first step in making sure of the reliability and efficiency of our method. The results obtained are in excellent agreement with those found by the usual density functional calculations by the DeMon program package. Advantages in computational time and storage have become significant with increasing the cluster size. This treatment has been applied to poly-water linear molecules as a model of ice cluster. The calculations were performed using $N_s=3$, 4 and 5 for investigating the size dependency of the starting cluster. The results obtained become more reliable with increasing the size of the starting cluster, while the calculations required for elongating one unit become more time consuming. The application to the water cluster has shown that $N_s=4$ is most reasonable in the view points of accuracy and efficiency. This treatment has also been applied to the two types of the structures (translational motif and screw axis motif) of formamide cluster. The energetic values, electron densities and overlap populations obtained did not show much differences between the two structures except for the increments in dipole moment. However, the tendency of the electron distribution on each unit was in the reverse of that of the water cluster.

In the present calculations, a few of examples for applications were demonstrated for examining applicability of our treatment. We did not elongate those clusters beyond several units because further elongation not only exceeds the limit of the capability of our computer, but also provides little additional information on regular polymers. In the small elongation within several units, therefore, the efficiency of our treatment may not be so significant compared to that of the direct LSD calculations using the DEMON program package. However, those results suggest that our treatment can be efficiently accessible to so large polymers that cannot be treated with the direct LSD calculations for the whole system.

ACKNOWLEDGMENTS

This work was supported by a grant from the Alexander-von-Humboldt Foundation. The authors thank Dr. Kieninger Martina for helpful discussions and encouragement. The present work was combined with her fast version of the deMon program package that she has improved in computational speed. The computations were carried out on a Convex 220 computer at the Rechenzentrum des Deutsches Krebsforschungszentrums.

[1] A. Imamura, Y. Aoki, and K. Maekawa, J. Chem. Phys. **95**, 5419 (1991).
[2] P. Hohenberg and W. Kohn, Phys. Rev. B **136**, 864 (1964).
[3] W. Kohn and L. J. Sham, Phys. Rev. A **140**, 1133 (1965).
[4] H. Sambe and R. H. Felton, J. Chem. Phys. **62**, 1122 (1975).
[5] B. I. Dunlap, J. W. D. Connolly, and J. R. Sabin, J. Chem. Phys. **79**, 3396 (1979).
[6] B. I. Dunlap, J. W. D. Connolly, and J. R. Sabin, J. Chem. Phys. **79**, 4993 (1979).
[7] D. R. Salahub, Adv. Chem. Phys. **69**, 474 (1987).
[8] A. St-Amant and D. R. Salahub, Chem. Phys. Lett. **169**, 387 (1990).
[9] Y. Aoki, S. Suhai, and A. Imamura, Int. J. Quantum Chem. (to be published).
[10] E. J. Baerends, D. E. Ellis, and P. Ros, Chem. Phys. **2**, 41 (1973).
[11] A. D. Becke, J. Chem. Phys. **84**, 2547 (1988).
[12] S. H. Vosko, L. Wilk, and M. Nasair, Can. J. Phys. **58**, 1200 (1980).
[13] L. Wilk and S. H. Vosko, J. Phys. C **15**, 2139 (1982).
[14] A. D. Becke, J. Chem. Phys. **85**, 7184 (1985).
[15] J. P. Perdew, Phys. Rev. B **33**, 8822 (1986).